Chapter 3

Process and Device Characterizations of Low-Temperature Polycrystalline Silicon-Germanium (poly-$Si_{1-x}Ge_x$) Thin Film Transistors

----

3.1 Introduction

Low-temperature polycrystalline silicon (LTPS) thin-film transistors have been widely studied because of their potential applications in high-performance displays, such as active matrix liquid crystal displays (AMLCDs) [3.1] – [3.7] and active matrix organic light emitting displays (AMOLEDs) [3.8] – [3.14]. When we consider the increasing display size and tight pixel density in future high-performance displays, LTPS TFTs with higher mobility are required in order to shorten the charging time of each pixel capacitor while keeping the same device size. To achieve high mobility for high-speed operation, excimer laser crystallization (ELC) has been widely adopted to enlarge the grain size and reduce the intragrain defect density due to the solidification of melted Si thin film [3.15] – [3.16]. The technique yields high-performance, glass substrate poly-Si TFTs with high throughput thanks to the large beam size of the high energy beam used. In addition, because this technique is of extremely short duration (100ns) and an large absorption coefficient for a-Si in the UV light

region of excimer laser, it can prevent the introduction of thermal damage to the glass substrate and there also is no need to worry about the thermal compaction problem, which is a serious issue in the solid phase crystallization method. However, the driving capability of LTPS TFT is restricted by other harmful factors such as huge surface roughness [3.17] – [3.18] and limited grain size under conventional excimer laser irradiation. Thus, substitutional fabrication methods must be provided to solve the disadvantages mentioned above.

Recently, many compound materials have been adopted as the channel material to improve the device properties [3.19] – [3.22]. Among them, the polycrystalline silicon-germanium (poly-$Si_{1-x}Ge_x$) thin film seems to be an excellent candidate for the channel active layer because of the high carrier mobility of Ge atom [3.23] – [3.28]. Poly-$Si_{1-x}Ge_x$ thin film has been widely used in nowadays high-performance semiconductor devices, such as metal-oxide-semiconductor field-effected transistors (MOSFETs) [3.29] – [3.31], heterojunction bipolar transistors (HBTs) [3.32] - [3.35], and high electron mobility transistors (HEMTs) [3.36] – [3.38].

For high speed device application, the $Si_{1-x}Ge_x$ layer is epitaxially grown on Si substrate as the base region in HBTs [3.39]. The device performance of $Si_{1-x}Ge_x$ HBTs can be greatly improved over the conventional Si bipolar transistor because the base region can be doped with much larger dopant concentration, which reduces the base resistivity and the resistance-capacitance (RC) time constant for device switching. The heterojunction discontinuity between the base and the emitter region resulting from the reduced bandgap of the $Si_{1-x}Ge_x$ base region suppresses the hole injection into the emitter region. Therefore, the current grain of the HBT would increase due to the reduction of hole injection.

For gate engineering, the work function of the poly-$Si_{1-x}Ge_x$ gate electrode can be adjusted with different Ge atomic concentration. This makes it become possible to replace the poly-Si gate electrode with poly-$Si_{1-x}Ge_x$ in CMOS technology. It has been demonstrated that

device performance was improved with poly-$Si_{1-x}Ge_x$ gate electrode due to lower resistivity, reduced gate depletion, and boron penetration [3.40].

On the other hand, for source/drain engineering, $Si_{1-x}Ge_x$ could also be adopted as a diffusion-source for the formation of shallow junction. In addition, it also has been shown that $Si_{1-x}Ge_x$ source/drain structure could suppress the short channel effect of submicron MOSFETs due to the valence band discontinuity cause by $Si_{1-x}Ge_x$ [3.41].

For channel engineering, Si/$Si_{1-x}Ge_x$ heterostructures with strained $Si_{1-x}Ge_x$ or strained Si [3.42] have attracted much attention recently because of the carrier mobility enhancement and the compatibility with nowadays Si technology. It has been demonstrated that MOSFETs with strained $Si_{1-x}Ge_x$ channel layer exhibited enhanced carrier mobility and superior device performance. The possible reason of the enhanced mobility could be attributed to higher in-plane carrier mobility of biaxially strained $Si_{1-x}Ge_x$ due to the reduction of interband carriers scattering in the valence band, where band-edge degeneracy was lifted by the strain.

In recent, low temperature poly-$Si_{1-x}Ge_x$ thin film transistors (LTPSG TFTs) also have been studied due to the lower process temperature of $Si_{1-x}Ge_x$ in comparison with Si [3.19] – [3.22]. Indeed, the lower melting temperature of Ge (1211 K) compared with Si (1683 K) means that poly-$Si_{1-x}Ge_x$ alloys have lower processing temperature. Several key fabrication processes, such as thin film deposition [3.43], thin film crystallization [3.44], and dopant activation can be carried out at lower temperature [3.45]. It seems also possible to decrease the thermal budget and improve, potentially, the electrical properties by incorporating germanium content in the silicon layers without modifying the existing Si-based processes. Poly-$Si_{1-x}Ge_x$ thin film can be acquired by direct deposition or recrystallization of a-$Si_{1-x}Ge_x$ thin film [3.27]. Direct deposition of poly-$Si_{1-x}Ge_x$ thin film has commonly been performed in a low pressure chemical vapor deposition (LPCVD) system typically at temperatures in the region of 550°C. For $Si_{1-x}Ge_x$ thin film deposition comparable growth rates to Si thin film can be obtained at lower temperatures while a higher Ge concentration results in higher growth

rate. According to the previous reports [3.27], small grain size and a great deal of defects were observed for the direct-deposited poly-SiGe thin film. Therefore, low-temperature poly-$Si_{1-x}Ge_x$ thin film transistors fabricated by direct-deposited poly-$Si_{1-x}Ge_x$ thin film demonstrate degraded electrical characteristics.

Several solid phase crystallization methods, which have been used in low-temperature poly-Si technology, have also been adopted in the field of recrystallization of a-$Si_{1-x}Ge_x$ thin film. Among them, the most widely used methods are solid phase crystallization (SPC) and rapid thermal annealing (RTA). The time to crystallization in solid state resrystallization is determined by the rate of crystalline nuclei formation and the solid phase epitaxial growth rate. It has already been demonstrated that a higher Ge content results in a higher solid phase epitaxy and therefore decreases the time and/or temperature needed for crystallization [3.46]. In addition, a pure amorphous Si (a-Si) thin film crystallizes with a strong (111) texture while that of $Si_{1-x}Ge_x$ thin film crystallizes with a (311) texture suggesting that the solid phase crystallization mechanism is changed by incorporation of Ge [3.47]. TEM analysis of the crystallized film shows that the grain morphology of the pure Si is an elliptical and/or a dendrite shape with a high density of microtwins in the grains while that of the poly-$Si_{1-x}Ge_x$ is more or less equiaxed shape with a much lower density of defects. The solid phase crystallization mechanism changes from a twin-assisted growth mode to a random growth mode as the Ge concentration in the film is increased.

On the other hand, alternative liquid-phase ways of producing $Si_{1-x}Ge_x$ crystalline layers have recently been suggested, including laser mixing of pure germanium amorphous films deposited on a silicon substrate [3.48] and ion beam induced crystallization of deposited amorphous $Si_{1-x}Ge_x$ films [3.49]. Several types of lasers and different wavelengths were tested: a Q-switched ruby laser, a XeCl excimer laser, and an ArF excimer laser. Excimer laser crystallization has been proven to be the most promising method in the fabrication of low-temperature poly-Si thin film. Poly-Si thin film with large grain size can be

manufactured with suitable laser irradiation conditions, such as laser energy density lying in super lateral growth regime, increasing laser shot number, and raising substrate temperature. The crystallization mechanism of a-Si by excimer laser irradiation at various energy regimes has been described elsewhere [3.50] – [3.51]. Three major regimes can be identified based on the thin film microstructure as a function of the incident laser energy density. The detail crystallization mechanism has been described in chapter 2. Crystallization of a-$Si_{1-x}Ge_x$ alloys, at low temperature, in short time, using excimer laser irradiation has been investigated by other authors [3.52]. Furthermore, it is reported that pulsed laser-induced growth of poly-$Si_{1-x}Ge_x$ offers several advantages over alternative epitaxial processes [3.53].

In this chapter, the process parameters for the deposition of a-$Si_{1-x}Ge_x$ thin films on oxidized wafer by LPCVD are fist investigated. Then, the microstructure of excimer laser crystallized poly-$Si_{1-x}Ge_x$ thin film is analyzed followed with an investigation of the factors affecting the crystallized poly-$Si_{1-x}Ge_x$ thin film. The microstructure excimer laser crystallized poly-$Si_{1-x}Ge_x$ thin film is also compared with that of conventional excimer laser crystallized poly-Si thin film. Combining with the results acquired from different material analysis methods, the fundamental excimer laser crystallization mechanism of poly-$Si_{1-x}Ge_x$ thin film is established. In addition, low-temperature poly-$Si_{1-x}Ge_x$ TFTs are produced by excimer laser crystallization. The electrical characteristics of the resulting devices are then reviewed. The relationship between the Ge segregation and the electrical performance of low-temperature poly-$Si_{1-x}Ge_x$ TFTs is also investigated. Finally, the electrical characteristics of low-temperature poly-$Si_{1-x}Ge_x$ TFTs are compared with those of conventional ELC low-temperature poly-Si counterparts.

3.2 Experimental Procedure

3.2.1 a-$Si_{1-x}Ge_x$ Thin Film Deposition

In order to prepare the sample for a-$Si_{1-x}Ge_x$ thin film deposition, silicon dioxide (SiO_2) with a thickness of 1 μm was thermally growth on bare silicon wafers by furnace. These oxidized silicon wafers were used as the starting substrate in order to imitate the real glass substrate. Before deposition of a-$Si_{1-x}Ge_x$ thin film, a smooth initial Si layer, effectively a few monolayers thick, was deposited at 450° to improve the nucleation of $Si_{1-x}Ge_x$ on SiO_2. This kills the long incubation time found for a-$Si_{1-x}Ge_x$ thin film deposition on an oxide surface [3.54]. And then, $Si_{1-x}Ge_x$ thin films with a thickness of 500Å were deposited on the oxidized Si wafers by low-pressure chemical vapor deposition (LPCVD) at different deposition temperature and gas pressure in order to find out the optimum deposition conditions. The Ge atomic concentration in the as-deposited $Si_{1-x}Ge_x$ thin film was adjusted by varying the germane (GeH_4) to silane (SiH_4) gas flow ratio. Detailed deposition parameters were listed in the Table 3.1.

Several material analysis methods were adopted to investigate the characteristics of the as-deposited $Si_{1-x}Ge_x$ thin film. X-ray diffraction (XRD) analysis was used to verify the amorphous phase of the as-deposited $Si_{1-x}Ge_x$ thin film. The glancing angle between the incident x-ray beam and the a-$Si_{1-x}Ge_x$ thin film was 1°. The Ge atomic concentration of the as-deposited a-$Si_{1-x}Ge_x$ thin film was identified by Rutherford backscattering spectroscopy (RBS). The deposition rate was also investigated as a function of deposition temperature and precursor gas flow ratio.

Table 3.1. Detailed deposition parameters of LPCVD $Si_{1-x}Ge_x$ Thin Film

Temperature (°C)	Pressure (mTorr)	SiH_4 (sccm)	GeH_4 (sccm)
450	300	60	2 3 8 13 17
470	300	60	3 8 13

3.2.2 Excimer Laser Crystallization of a-$Si_{1-x}Ge_x$ Thin Film

For the excimer laser crystallization, a-$Si_{1-x}Ge_x$ thin film of a thickness of 500Å was used as the starting material. Before deposition of a-$Si_{1-x}Ge_x$ thin film, a smooth initial Si layer, effectively a few monolayers thick, was deposited at 450° to improve the nucleation of $Si_{1-x}Ge_x$ on SiO_2. This kills the long incubation time found for a-$Si_{1-x}Ge_x$ thin film deposition on an oxide surface. The a-$Si_{1-x}Ge_x$ thin film was deposited on the oxidized Si wafers by low-pressure chemical vapor deposition (LPCVD) at 450°C and 300mTorr, which were the optimum deposition conditions found in former work. The a-$Si_{1-x}Ge_x$ thin film was prepared by decomposition of pure germane (GeH_4) and silane (SiH_4). The substrates were cleaned employing a standard RCA-process before loading them into the deposition tube. The pulsed-KrF (248nm) excimer laser crystallization of a-$Si_{1-x}Ge_x$ thin film was carried out in vacuum ambient pumped down to ~10^{-3} Torr at room temperature or 400℃. The laser beam was homogenized into a top-flat profile in the long axis and the short axis was still maintained at a semi-gaussian profile. The scanning direction was along the short axis. The numbers of laser shot per unit area were 100 and 20, which were equivalent to the overlaps of 99% and 95% respectively.

Several material analysis techniques were used to investigate the relation between the morphology of crystallized poly-Si thin films and laser process conditions. The composition of the as-deposited a-$Si_{1-x}Ge_x$ layers was measured by Rutherford backscattering spectroscopy (RBS). X-ray diffractometry (XRD) measurements in the θ-2θ configuration were performed to determine the evolution of crystallization as well as the existence of preferred grain orientation as a function of excimer laser annealing conditions. The atomic bonding changes and the crystallinity of as-deposited $Si_{1-x}Ge_x$ film induced by the laser annealing were studied by Raman spectroscopy. The atomic depth profiles of the $Si_{1-x}Ge_x$ thin film before and after laser annealing were deduced from Auger electron spectroscopy (AES). Scanning electron microscopy (SEM) was utilized to analyze the grain structure and grain size. In order to facilitate the SEM observation, the samples were processed by Secco-etch before analysis. Secco-etch preferably etches the grain boundary in poly-$Si_{1-x}Ge_x$ thin film. Plan-view transmission electron microscopy (TEM) was used to determine the in-plan grain shape and size.

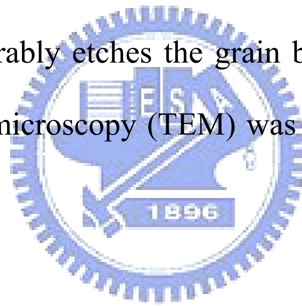
1896

3.2.3 Fabrication of Low-Temperature Poly-$Si_{1-x}Ge_x$ TFTs Using ELC

The procedure of fabricating top-gate, self-aligned p-channel poly-$Si_{1-x}Ge_x$ TFTs with excimer laser crystallization is illustrated in Figure 3.1. a-$Si_{1-x}Ge_x$ thin film with a 500Å thickness was first deposited on oxidized silicon substrate by low pressure chemical vapor deposition (LPCVD) at 450°C using SiH_4 and GeH_4 as gas precursors. The GeH_4 to SiH_4 gas flow ratio was adjusted to obtain a-$Si_{1-x}Ge_x$ thin films with different Ge atomic concentration. Before deposition of a-$Si_{1-x}Ge_x$ thin film, a smooth initial Si layer, effectively a few monolayers thick, was deposited at 450° by LPCVD to improve the nucleation of a-$Si_{1-x}Ge_x$

on SiO_2. This killed the long incubation time found for a-$Si_{1-x}Ge_x$ thin film deposition on an oxide surface. After clean process, the wafer was then subjected to 248nm KrF excimer laser annealing in a vacuum chamber pumped down 10^{-3} torr at room temperature. The laser beam was homogenized into a semi-gaussian shape in the short axis and a flat-top shape in the long axis. The laser energy density was controlled in the super lateral growth regime. The laser shot numbers per unit area were 100 in this work. After laser irradiation, poly-$Si_{1-x}Ge_x$ thin film was defined into individual active island. Next, 1000Å TEOS gate oxide was deposited by plasma-enhanced chemical vapor deposition (PECVD) at 385°C. A 3000Å aluminum film was then deposited by thermal evaporation. The Al was etched by hot phosphoric mixed acid and the gate oxide was etched by reactive ion etching (RIE) to form gate electrodes. After the gate electrodes were patterned, a self-aligned B^+ ion implantation with the dose concentration of 5×10^{15} cm^{-2} was carried out to form the source and drain regions. A 3000Å TEOS oxide was deposited by PECVD at 350°C as passivation layers. Then, excimer laser annealing was performed to activate the implanted dopants and recrystallize the source and drain region at room temperature. The shot numbers per unit area used for dopant activation were 20 and the laser energy density was controlled in the partial melting regime.. After contact holes opening, Al was deposited by thermal evaporation and patterned to form the electrical connecting pads. Finally, the devices were treated with NH_3 plasma by PECVD for four hours. The maximum process temperature of the ELC poly-$Si_{1-x}Ge_x$ TFTs fabrication was 450℃. Conventional ELC poly-Si TFTs were also fabricated for comparison.

The typical transfer and output characteristics of the ELC poly-$Si_{1-x}Ge_x$ TFTs were measured by HP4156 precise emiconductor parameter analyzer. The device parameters including field-effect mobility, threshold voltage, subthreshold swing and on/off current ratio were extracted from the measured characteristics. The electrical performances of the ELC poly-Si controlling samples were also estimated to compare with the ELC poly-$Si_{1-x}Ge_x$ counterparts.

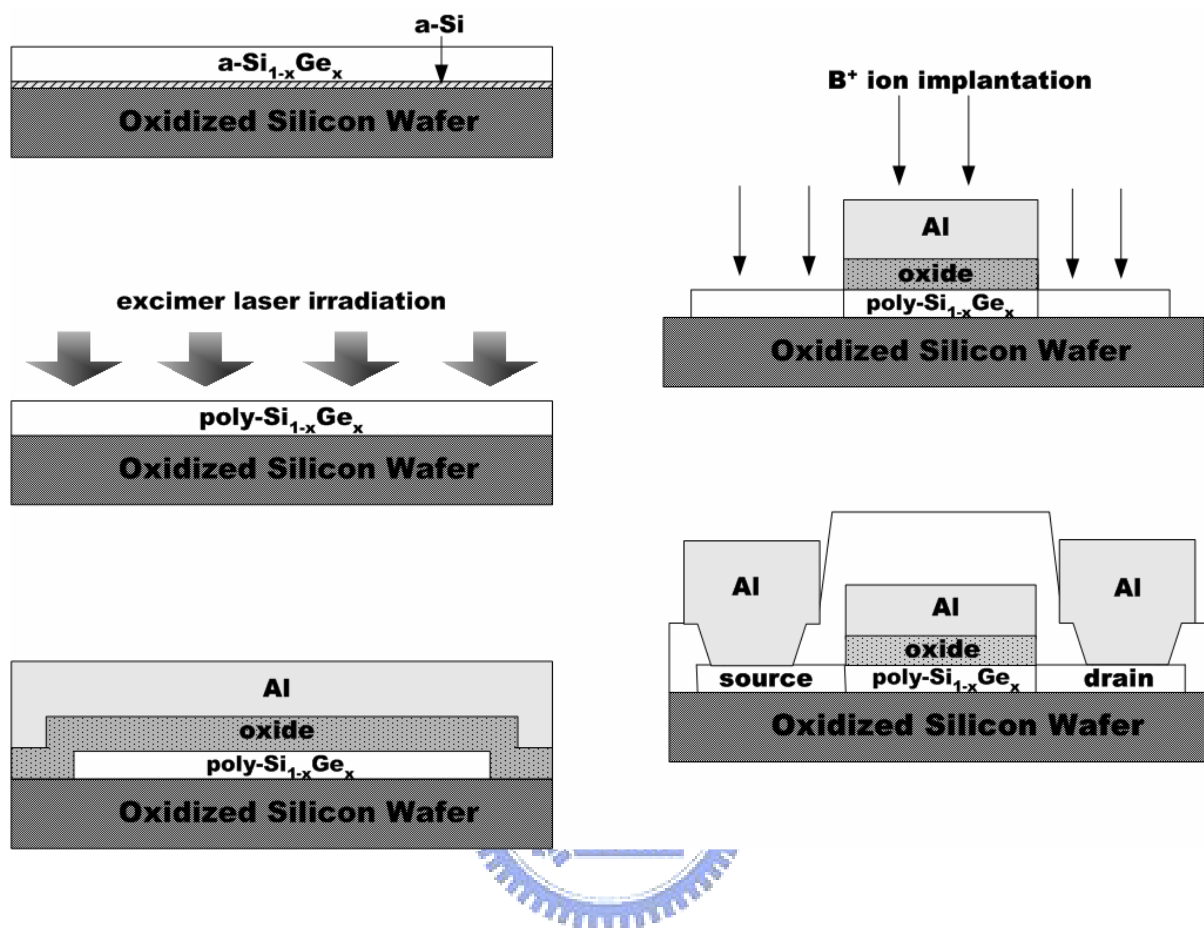

Figure 3.1. The key process procedure of fabricating ELC poly-$Si_{1-x}Ge_x$ TFTs.

3.3 Material Characterization of $Si_{1-x}Ge_x$ Thin Films

3.3.1 Deposition Characterization of a-$Si_{1-x}Ge_x$ Thin Films

It has been well documented that the thermal budget of $Si_{1-x}Ge_x$ alloy is much less than that of the pure Si film. Indeed, this has been one of the major motivations for using the $Si_{1-x}Ge_x$ alloy layer as an active layer for TFTs. A-$Si_{1-x}Ge_x$ thin film can be acquired at

different pressure and temperature by a variety of techniques, including molecular beam epitaxy (MBE), sputtering, Ge ion implantation, ultra-high vacuum chemical vapor deposition (UHVCVD), plasma-enhanced chemical vapor deposition (PECVD), rapid thermal chemical vapor deposition (RTCVD), and low-pressure chemical vapor deposition (LPCVD)…etc. Among these deposition methods, the a-$Si_{1-x}Ge_x$ alloy all demonstrates a lower deposition temperature compared to a-Si films. It has also been reported that the growth rate of the a-$Si_{1-x}Ge_x$ thin film was higher than that of a-Si thin film, and the growth rate increased with Ge atomic concentration.

In this work, the deposition of a-$Si_{1-x}Ge_x$ thin films was performed in a conventional hot wall LPCVD system using silane (SiH_4) and germane (GeH_4) as the gaseous source. The deposition temperature was controlled below 460°C to maintain the amorphous phase of the as-deposited $Si_{1-x}Ge_x$ thin film while the deposition temperature of a-Si was kept at 550°C. The total deposition reaction sequence is listed as following:

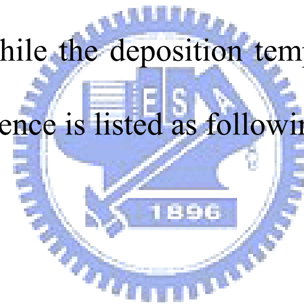

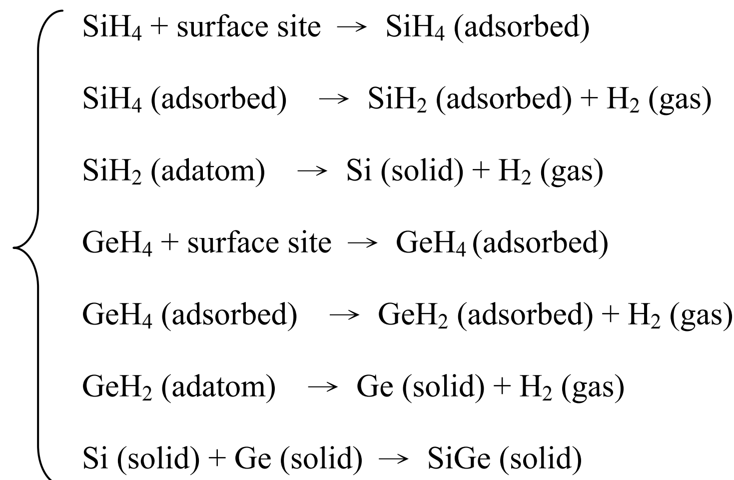

$$\begin{cases} SiH_4 + \text{surface site} \rightarrow SiH_4\ (\text{adsorbed}) \\ SiH_4\ (\text{adsorbed}) \rightarrow SiH_2\ (\text{adsorbed}) + H_2\ (\text{gas}) \\ SiH_2\ (\text{adatom}) \rightarrow Si\ (\text{solid}) + H_2\ (\text{gas}) \\ GeH_4 + \text{surface site} \rightarrow GeH_4\ (\text{adsorbed}) \\ GeH_4\ (\text{adsorbed}) \rightarrow GeH_2\ (\text{adsorbed}) + H_2\ (\text{gas}) \\ GeH_2\ (\text{adatom}) \rightarrow Ge\ (\text{solid}) + H_2\ (\text{gas}) \\ Si\ (\text{solid}) + Ge\ (\text{solid}) \rightarrow SiGe\ (\text{solid}) \end{cases}$$

For $Si_{1-x}Ge_x$ deposition onto an amorphous oxide surface, there are two factors that contribute to the long incubation time for nucleation on the oxide. One is the lack of low energy surface sites on an amorphous oxide surface, and the other is the formation of volatile GeO species at the early stage of the nucleation [3.55]. Deposition pressure and temperature also play an important role in $Si_{1-x}Ge_x$ nucleation on oxides. Low deposition pressure tends to reduce the impinging rate of gas species onto the oxide, thus increasing the incubation time while low deposition temperature reduces the atomic migration energy on the oxide leading to a decrease in nucleation rate. To circumvent the partial selectivity problem in order to use $Si_{1-x}Ge_x$ alloys as the gate material in CMOS technology, several approaches have been made to nucleate poly- $Si_{1-x}Ge_x$ on the oxide such as Si predeposition [3.56] – [3.57] and plasma sputtering of the oxide surface [3.58] – [3.59]. In this study, to overcome the nucleation problem of the deposition of a-$Si_{1-x}Ge_x$ thin film on SiO_2, a thin seed Si layer was pre-deposited on SiO_2 surface by exposing the SiO_2 to SiH_4 gas for a short time. The thin Si film deposition (Si flash technique) on oxide was intended to provide adequate nucleation sites on the oxide surface for subsequent growth of a-$Si_{1-x}Ge_x$ thin film

To examine the crystalline phase of the as-deposited $Si_{1-x}Ge_x$ thin film, x-ray diffraction (XRD) was performed on these samples acquired from different deposition parameters. Figure 3.2 is the XRD results of the as-deposited $Si_{1-x}Ge_x$ thin films with different deposition parameters. The detail relationships between the deposition parameters and the eventual crystalline phase are listed in Table 3.2. The result shows that the $Si_{1-x}Ge_x$ thin films deposited at 450℃ display a pure amorphous phase under three different gas flow ratios. Thus, 450˚C seems to be an optimum deposition temperature to fabricate a-$Si_{1-x}Ge_x$ thin film by LPCVD.

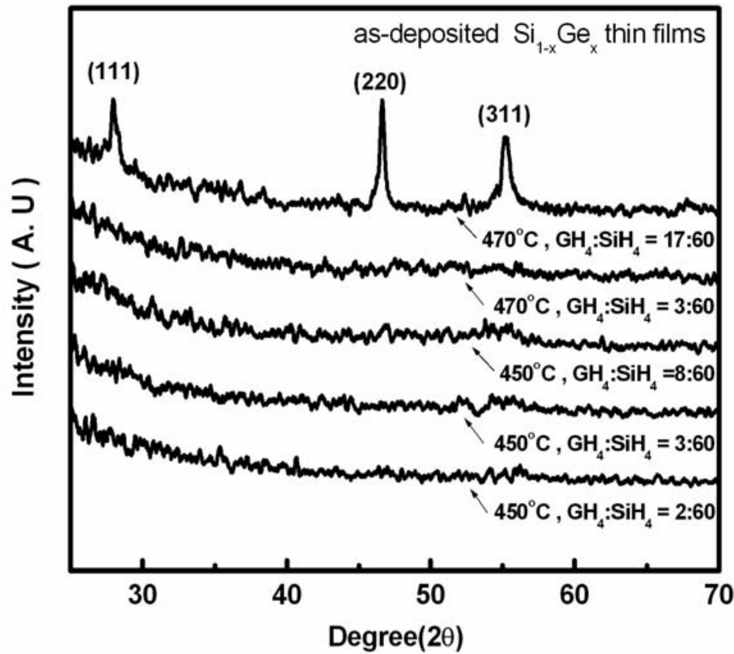

Figure 3.2. XRD spectrum of as-deposited LPCVD $Si_{1-x}Ge_x$ thin film.

It has been reported that the as-deposited poly-$Si_{1-x}Ge_x$ thin films were found to exhibit singular peaks at around 2θ=28°, 47°, and 55° in XRD spectra. It is corresponding to the {111}, {220}, and {311} planes, which are indicator of diamond-cubic crystal structure. As shown in Fig. 3.1, three obvious peaks can be found for the $Si_{1-x}Ge_x$ thin film deposited at 470˚C with a 17:60 GeH_4 to SiH_4 gas ratio. This means that under this deposition condition, the as-deposited $Si_{1-x}Ge_x$ thin film displays a polycrystalline phase. As the deposition temperature increases, the crystalline phases of the as-deposited $Si_{1-x}Ge_x$ thin films tend to change from amorphous state to polycrystalline state. The transition temperature between amorphous phase and polycrystalline phase also becomes higher as the GeH_4 gas flow rate increases. Such a result is consistent with the research reported previously. In addition, a maximum peak intensity occurs in the {220} texture. It is attributed to the partial hydrogen coverage of silicon surface promoting the {220} grain growth.

Table 3.2. The detail relationship between the deposition parameters and the crystalline phase.

A: amorphous phase, P: polycrystalline phase

Temperature (°C)	SiH_4 (sccm)	GeH_4 (sccm)	Deposition rate (Å/min)	Ge fraction	Phase
450	60	2	4.17	23	A
		3	6.86	33	A
		8	14.73	42	A
		13	21.18	N/A	P
		17	27.98	N/A	P
470	60	3	8.45	26	A
		8	17.4	36	A
		13	26.6	41	P

The relationship between the deposition rate and Ge atomic concentration of a-$Si_{1-x}Ge_x$ thin films are shown in Figure 3.3, where the Ge atomic concentration is determined by Rutherford Backscattering Spectroscopy (RBS) analysis. As depicted in Figure 3.3, the deposition rate is a function of deposition temperature and Ge atomic concentration in the a-$Si_{1-x}Ge_x$ thin film. The deposition rate is enhanced as the Ge atomic concentration in the a-$Si_{1-x}Ge_x$ thin film increases. The germane precursor has an enormous catalytic effect on the growth rate of silicon at low temperatures. This could be attributed to that germane acts as a catalyst to enhance hydrogen desorption from the deposition surface [3.60]. Since the deposition conditions in this study are controlled in the surface-reaction-limited regime, the deposition rate is restricted by hydrogen desorption rate at the film surface. The hydrogen desorption energy is apparently reduced when more Ge atoms ware incorporated during a-$Si_{1-x}Ge_x$ thin film deposition due to the weaker Ge-H bond (comparing the +90.79 kJ/moe enthalpy of formation for germane to the +32.64 kJ/mol value for silane). Therefore, the deposition rate of a-$Si_{1-x}Ge_x$ thin film will increase with germane precursor gas flow rate.

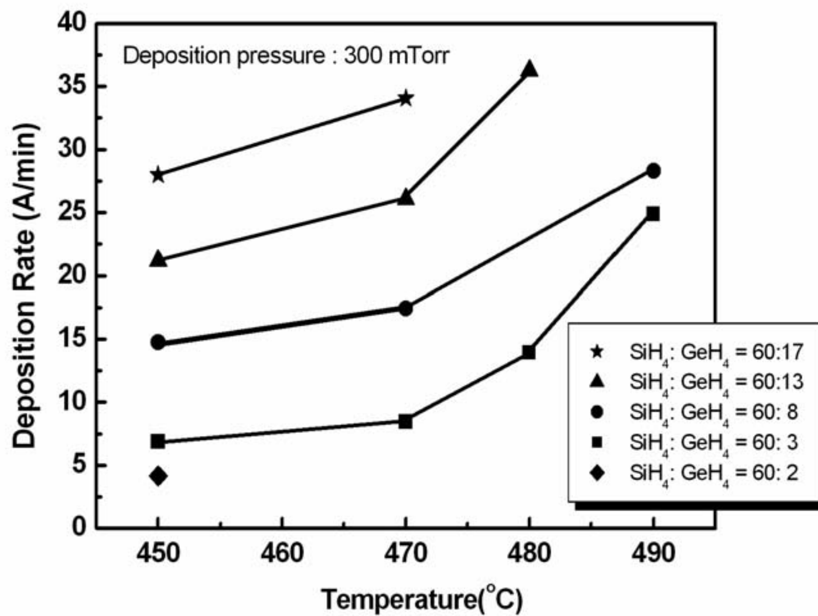

Figure 3.3. $Si_{1-x}Ge_x$ thin film deposition rate as a function of temperature with different SiH_4/GeH_4 gas flow ratio.

Figure 3.4 displays the relationship between the Ge atomic concentration in the as-deposited a-$Si_{1-x}Ge_x$ thin film and GeH_4/SiH_4 gas flow ratio for two different deposition temperatures (450℃ and 470℃). Under a fixed gas flow ratio, the Ge atomic fraction in the $Si_{1-x}Ge_x$ thin film increases as the deposition temperature decreases. The phenomenon may be ascribed to the different sticking coefficients of Si and Ge atoms on the oxide. For CVD system, the following five steps are fundamental to all processes: 1) the reactants are transported to the substrate surface; 2) the reactant are adsorbed on the substrate surface; 3) a chemical reaction takes place on the surface leading to the formation of the film and reaction products; 4) the reaction products are desorbed from the surface; and 5) the products are transported away from the surface. The step of reactant adsorption on the substrate surface is related to the sticking coefficient of the reactants. Thus the sticking coefficient of the reactant becomes one of the dominant parameters during thin film deposition. The growth rate can be enhanced with large sticking coefficient. In this case, under higher deposition temperature,

the sticking coefficient of Si precursor increases more rapidly than that of Ge precursor. More Si atoms are absorbed on the film surface at elevated deposition temperature. As a result, less Ge atoms will be included in the as-deposited a-$Si_{1-x}Ge_x$ thin film when deposition temperature raises, which results in a decreasing Ge atomic concentration.

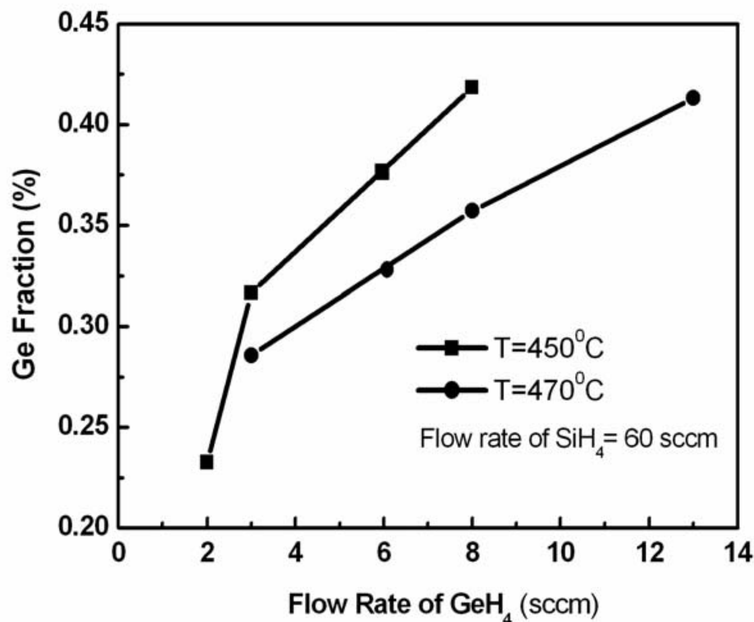

Figure 3.4. The relationship between the Ge atomic concentration and GeH_4/SiH_4 gas flow ratio for two deposition temperatures of 450℃ and 470℃.

3.3.2 Material Characterization of ELC poly-$Si_{1-x}Ge_x$ thin film

3.3.2.1 X-ray Diffraction (XRD) Analysis

X-ray diffraction (XRD) measurements in the θ - 2θ configuration were performed to determine the evolution of crystallization as a function of laser irradiation conditions as well as the existence of preferred grain orientations, the grain size in the depth direction and the crystallinity of the poly-$Si_{1-x}Ge_x$ thin films. Figure 3.5 and Figure 3.6 display the XRD

spectra of poly-$Si_{1-x}Ge_x$ thin films crystallized with different laser energy at room temperature. The shot numbers per unit area are 100. The Ge atomic concentrations of the poly-$Si_{1-x}Ge_x$ thin films are 23% and 33%, respectively. The diffraction peaks appearing at around $2\theta = 28^{\circ}$, 47°, and 55° represent the diffraction peaks from the (111), (220), and (311) planes, respectively. This suggested the $Si_{1-x}Ge_x$ thin film deposited in an amorphous state can be effectively converted to polycrystalline state after excimer laser irradiation. In addition, the x-ray diffraction peaks of the ELC poly-$Si_{1-x}Ge_x$ thin film locate between the theoretical angles of the randomly oriented pure poly-Si and pure poly-Ge thin films. No separate (311) Si and Ge peaks, which relates to the formation of clusters, are observed in this work. As a result, the ELC poly-$Si_{1-x}Ge_x$ alloys are formed rather than Ge clusters existing within a matrix of Si grains, or vice versa. On the other hand, no dominant peak is inspected for the ELC poly-$Si_{1-x}Ge_x$ thin film. This means that the ELC poly-$Si_{1-x}Ge_x$ thin film is composted of grains with a random crystalline orientation.

E S A
1896

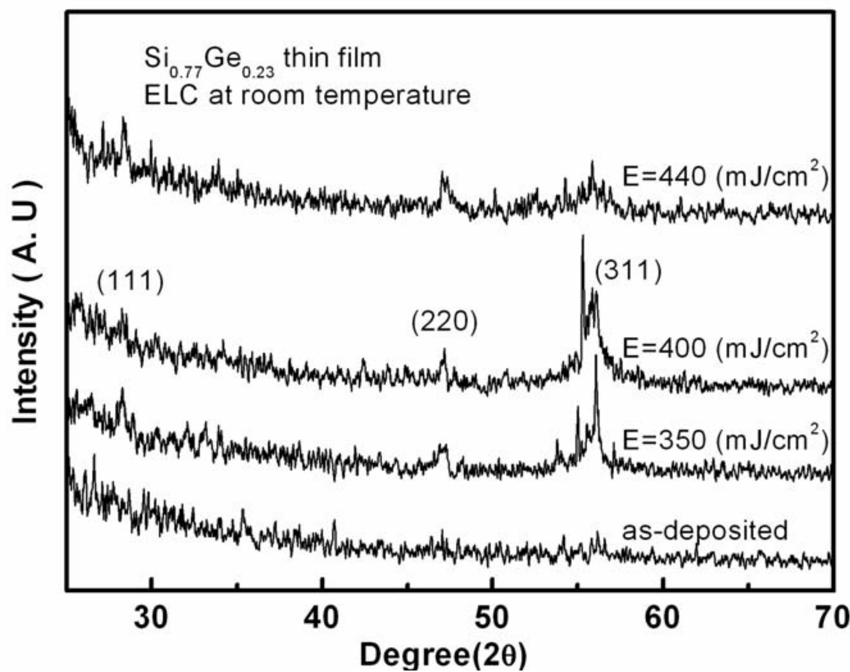

Figure 3.5. XRD spectrum of ELC $Si_{0.77}Ge_{0.23}$ thin film irradiated at room temperature.

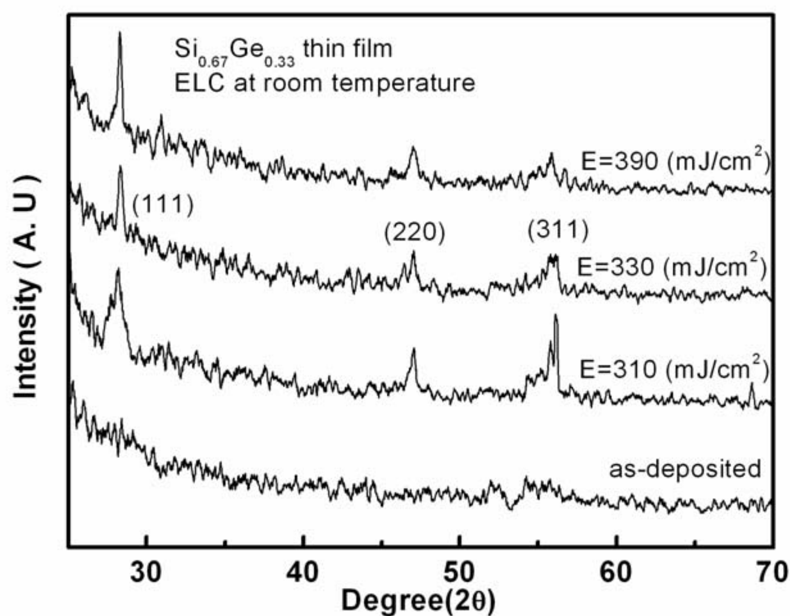

Figure 3.6. XRD spectrum of ELC $Si_{0.67}Ge_{0.33}$ thin film irradiated at room temperature.

Figure 3.7 shows the XRD spectra of ELC poly-$Si_{0.77}Ge_{0.23}$ thin films irradiated at 400°C with shot densities of 20 and 100. The intensities of the three diffraction peaks become more obvious owing to the better crystallinity resulting from the substrate heating, which is consistent with the crystallization mechanism mentioned in chapter 2.

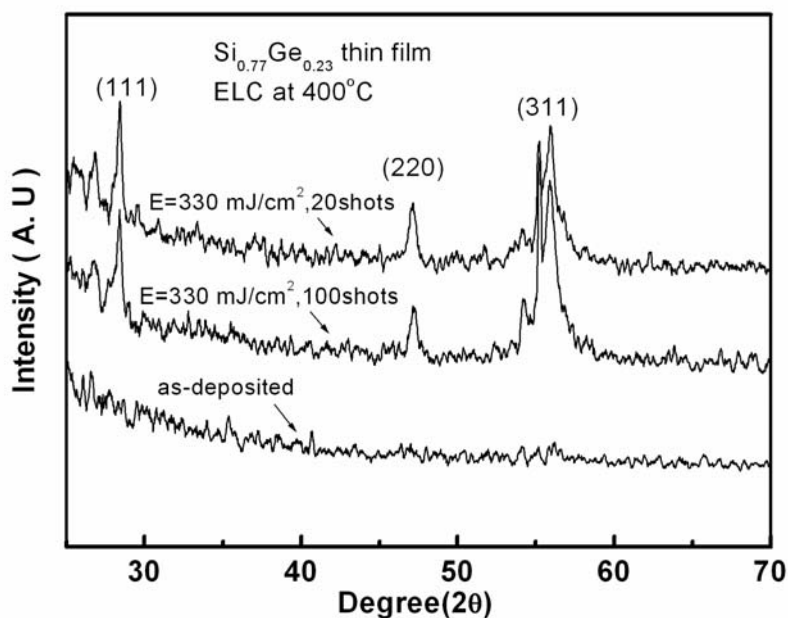

Figure 3.7. XRD spectrum of ELC $Si_{0.77}Ge_{0.23}$ thin film irradiated at 400°C.

3.3.2.2 Raman Spectroscopy Analysis

Raman spectroscopy is a contactless technique providing information about all these features in $Si_{1-x}Ge_x$ thin film with a high degree of experimental simplicity. It has been proven to be sensitive to the composition, stress and phonon correlation length. The crystalline volume fraction of the polycrystalline thin film can also be obtained from de-convoluting the Raman spectrum of the polycrystalline thin film into crystalline and amorphous components. Figure 3.8 and Figure 3.9 is the Raman spectra of the crystallized poly-$Si_{1-x}Ge_x$ thin films irradiated with different laser energy at room temperature. The shot numbers per unit area are 100. As shown in these figures, the broad band of the as-deposited $Si_{1-x}Ge_x$ thin film represents no crystalline phase existing inside the film. In addition, the Raman peak intensity of the Si substrate is weak due to the strong absorption coefficient of a-$Si_{1-x}Ge_x$ thin film at the wavelength of incident Raman laser beam. After excimer laser irradiation, the absorption coefficient of the poly-$Si_{1-x}Ge_x$ thin film decreased. Thus, the poly-$Si_{1-x}Ge_x$ thin film becomes more transparent and the intensity of the characteristic first order Raman band of the Si substrate at 520cm^{-1} grows into evidence. In the mean time, three main peaks around at 300, 400 and 500 cm^{-1}, are observed. The three peaks were corresponding to Ge-Ge, Si-Ge, and Si-Si bonds with zone edge phonons vibration mode, respectively. This is in agreement with the previous XRD analysis results, which the poly-$Si_{1-x}Ge_x$ alloy was formed instead of Ge clusters. The Raman peak intensity increase to a maximum count when the applied laser energy density reaches certain value, and then decreases as laser energy density further increase. The deviation in the optimum laser energy density for poly-$Si_{0.77}Ge_{0.23}$ and poly-$Si_{0.67}Ge_{0.33}$ thin film may be ascribed to the difference in the excimer laser absorption coefficient as the Ge atomic concentration varies. The tendency of Raman spectra for the ELC poly-$Si_{1-x}Ge_x$ thin film is consistent with that for ELC poly-Si counterpart. This means the laser crystallization mechanism of poly-$Si_{1-x}Ge_x$

thin film is similar to that of poly-Si thin film mentioned in chapter 2.

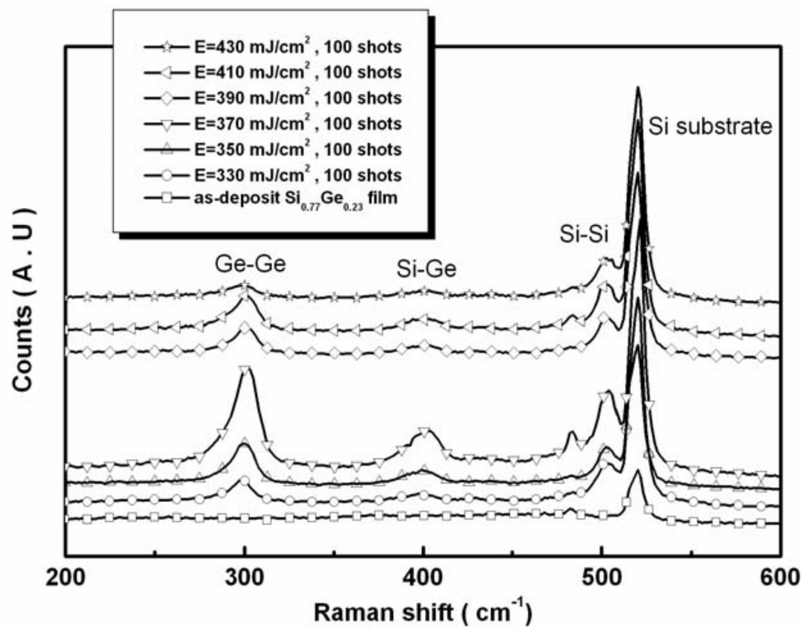

Figure 3.8. Raman spectra of ELC $Si_{0.77}Ge_{0.23}$ thin films irradiated with different laser energy density at room temperature.

1896

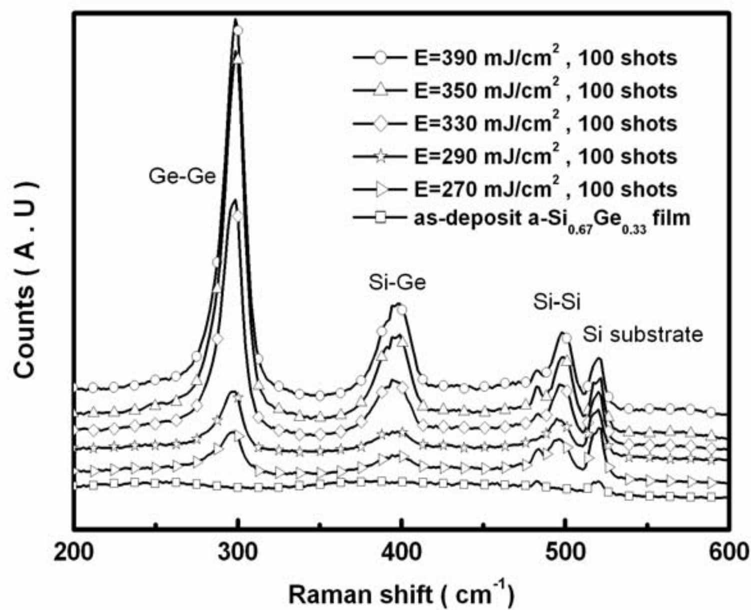

Figure 3.9. Raman spectra of ELC $Si_{0.67}Ge_{0.33}$ thin films irradiated with different laser energy density at room temperature.

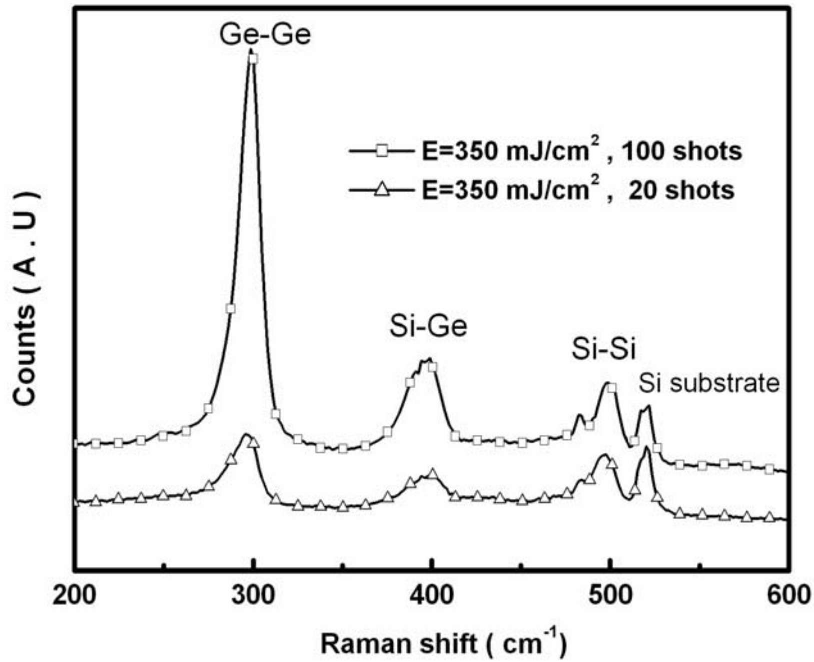

Figure 3.10 Raman spectra of ELC $Si_{0.67}Ge_{0.33}$ thin films irradiated with different shot numbers at room temperature. The laser energy density is 350 mJ/cm^2.

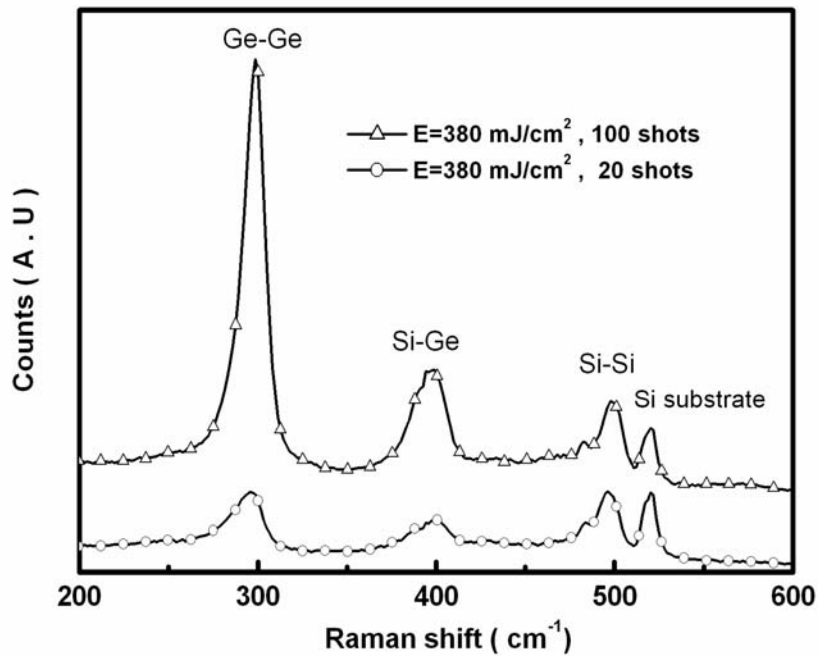

Figure 3.11 Raman spectra of ELC $Si_{0.67}Ge_{0.33}$ thin films irradiated with different shot numbers at room temperature. The laser energy density is 380 mJ/cm^2.

The peaks in Raman spectra is derived from k=0 phonon modes of the polycrystalline material. Therefore, a sharper Raman peak with great intensity implies an improvement in the crystallinity of the thin film. Figure 3.10 and Figure 3.11 show the Raman spectrum of the ELC poly-$Si_{1-x}Ge_x$ thin film irradiated with different laser shot numbers. As expected, the crystallinity of the two ELC poly-$Si_{1-x}Ge_x$ thin films are ameliorated with increasing laser shot numbers. This also agrees with the results of ELC poly-Si thin film.

3.3.2.3 Auger Electron Spectroscopy (AES) Analysis

Auger electron spectroscopy (AES) measurements were performed to investigate the Si and Ge depth profiles of the as-deposited a-$Si_{1-x}Ge_x$ thin film and the ELC poly-$Si_{1-x}Ge_x$ thin film as a function of laser irradiation conditions. Figure 3.12 displays the depth profile of the as-deposited a-$Si_{1-x}Ge_x$ thin film. Obviously, it can be found that the Si and Ge atoms are distributed uniformly in the as-deposited $Si_{1-x}Ge_x$ thin film.

On the other hand, Figure 3.13 ~ Figure 3.17 show the depth profile of Si and Ge concentration in the $Si_{1-x}Ge_x$ thin film after excimer laser irradiation with different laser shot numbers and laser energy densities at room temperature. In this case, for the sake of simplicity, only the ELC $Si_{0.77}Ge_{0.23}$ thin films were used for comparison. This is a universal result for other ELC $Si_{1-x}Ge_x$ thin films. As shown in these figures, it can be seen that, after excimer laser irradiation, the Si and Ge depth profiles are strongly modified with a redistribution of the Si and Ge atoms near the film surface. More Ge atoms are segregated to the film surface after laser irradiation while the Si surface concentration is reduced. This phenomenon becomes more noticeable as the total numbers of laser shot and/or the applied laser energy density increases. This means that the atom redistribution phenomenon is proportional to the total melting period during excimer laser crystallization. The segregation

of the Ge atom may be related to a non-equilibrium phase process that occurs during the rapid solidification of the laser-irradiated $Si_{1-x}Ge_x$ thin film. Due to the higher melting point of Si compared to Ge, the Si atoms in the melting $Si_{1-x}Ge_x$ thin film will be expected to solidify first. Therefore, lots of retained-liquid Ge atoms will progress along with the liquid/solid interface in the laser-irradiated $Si_{1-x}Ge_x$ thin film. At the end of solidification, numerous Ge atoms aggregate at the film surface, where is the last solidification region during excimer laser crystallization.

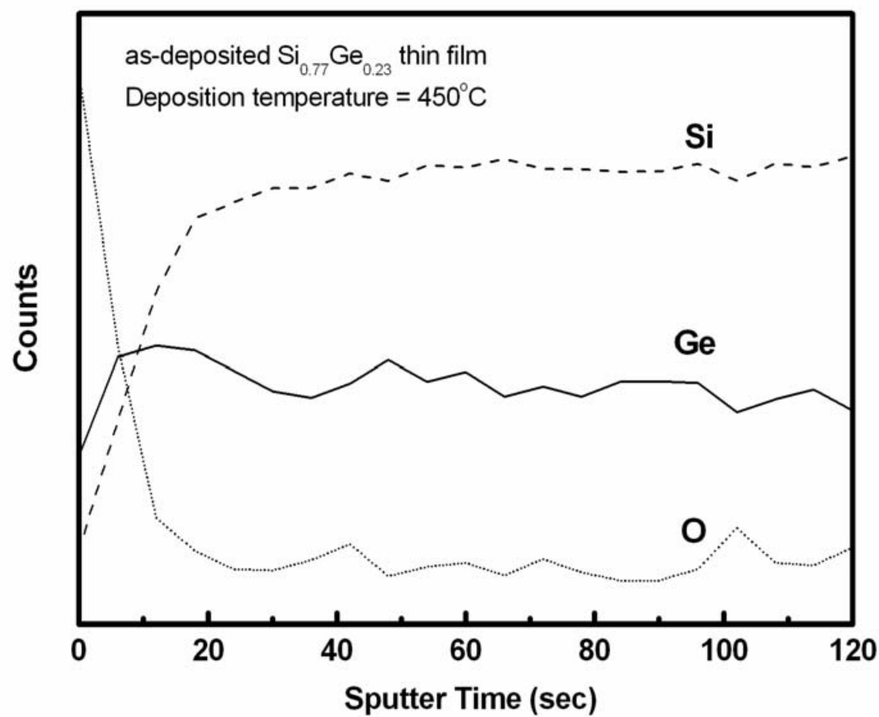

Figure 3.12. AES depth profile of the as-deposited a-$Si_{0.77}Ge_{0.23}$ thin film.

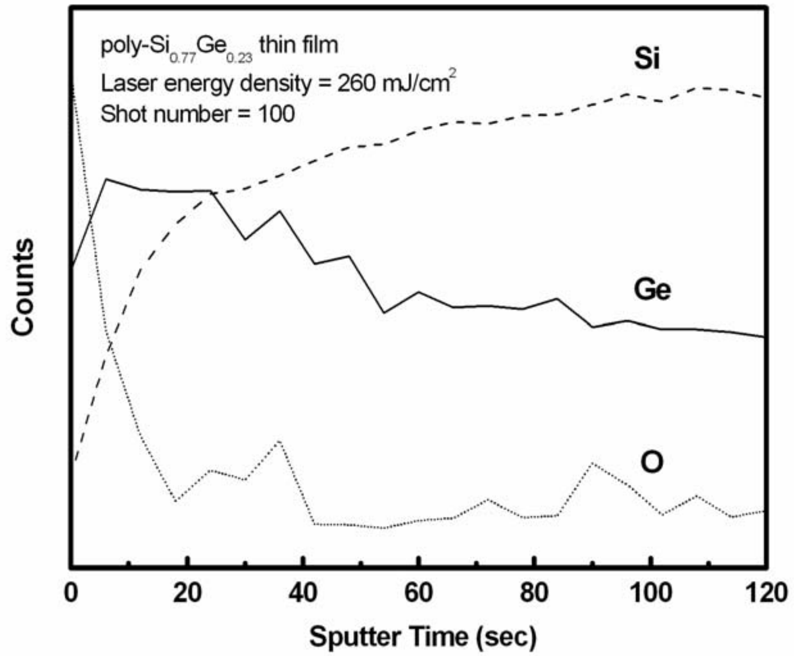

Figure 3.13. AES depth profile of the ELC poly-$Si_{0.77}Ge_{0.23}$ with E = 260 mJ/cm^2, 100 shots at R.T.

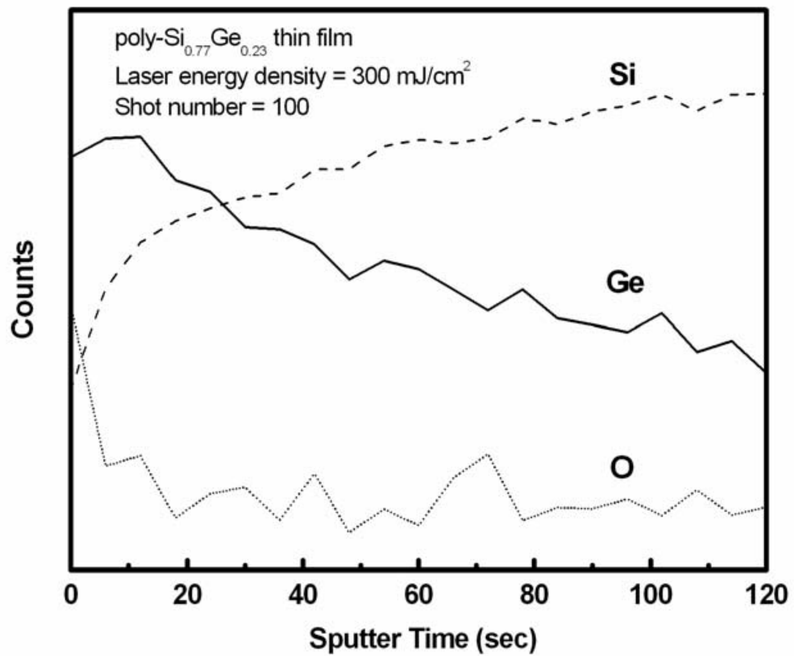

Figure 3.14. AES depth profile of the ELC poly-$Si_{0.77}Ge_{0.23}$ with E = 300 mJ/cm^2, 100 shots at R.T.

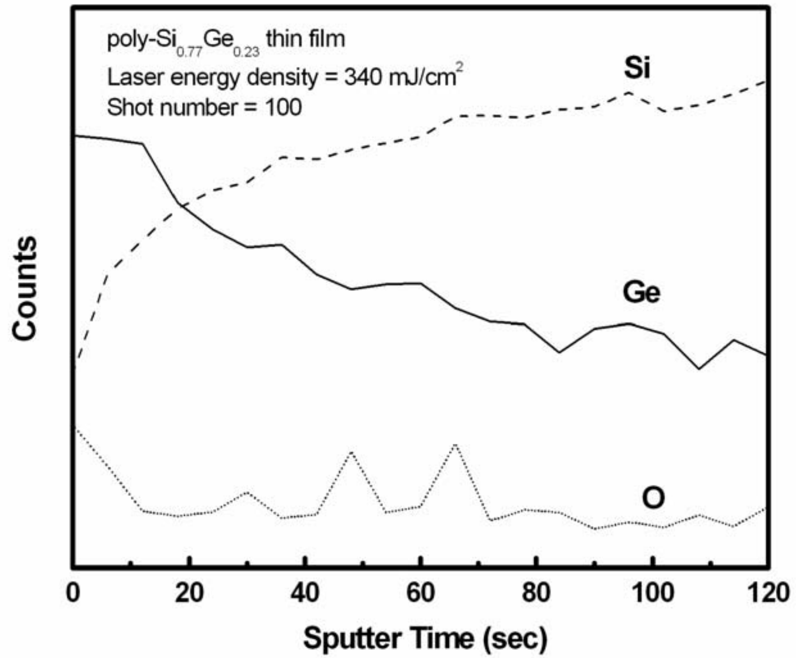

Figure 3.15. AES depth profile of the ELC poly-$Si_{0.77}Ge_{0.23}$ with E = 340 mJ/cm^2, 100 shots at R.T.

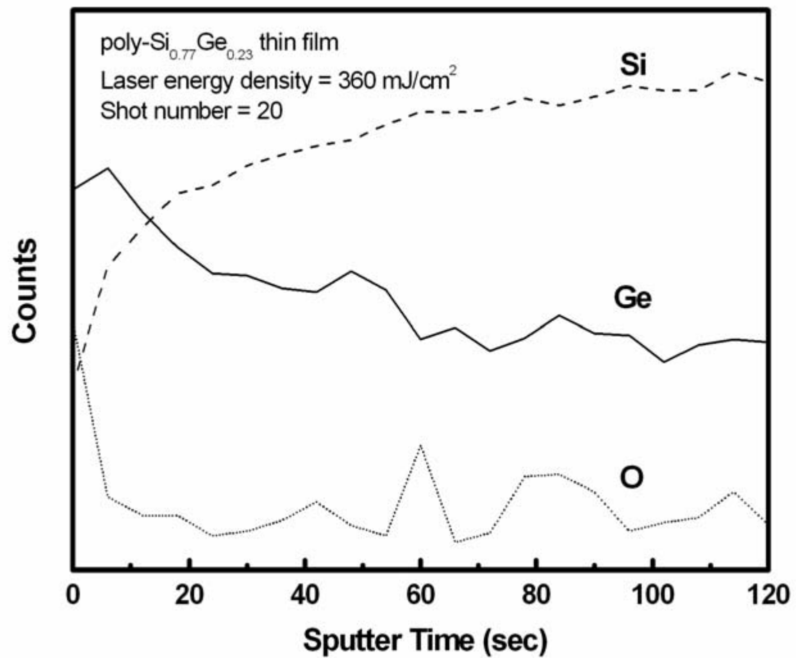

Figure 3.16. AES depth profile of the ELC poly-$Si_{0.77}Ge_{0.23}$ with E = 360 mJ/cm^2, 20 shots at R.T.

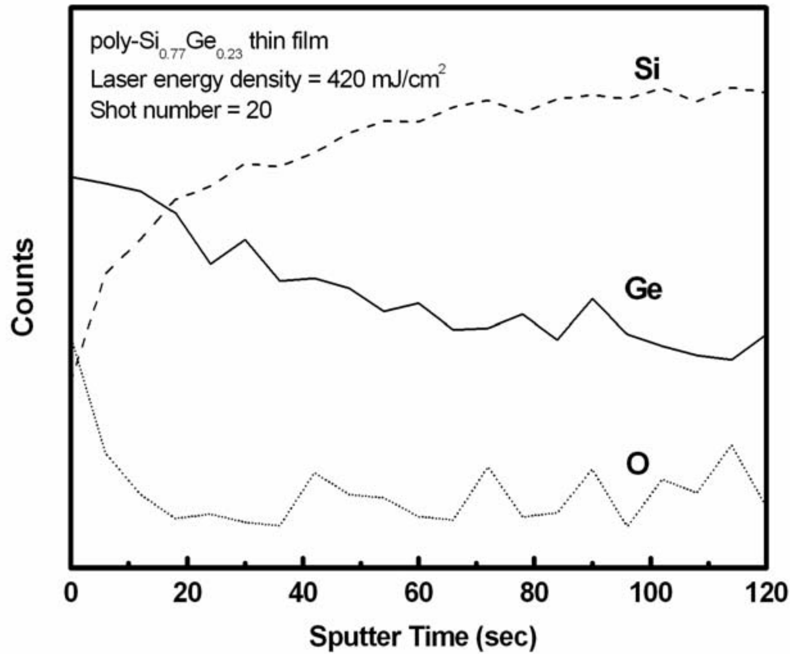

Figure 3.17. AES depth profile of the ELC poly-$Si_{0.77}Ge_{0.23}$ with E = 420 mJ/cm^2, 20 shots at R.T.

3.3.2.4 Transmission Electron Microscopy (TEM) Analysis

The micro-structural morphologies such as the grain size, inter- and intra-grain defect density, and grain orientation can be investigated by using Transmission Electron Microscopy (TEM) and its electron diffraction patterns. In order to analysis for convenience, a-$Si_{0.77}Ge_{0.23}$ thin films prepared by ultra-high vacuum chemical vapor deposition (UHVCVD) were adopted. The deposition temperature was 450°C and the precursors were mixed of silane and germane, which were the same as those for LPCVD system. Before deposition of a-$Si_{0.77}Ge_{0.23}$ thin film, a smooth initial Si layer, effectively a few monolayers thick, was also deposited at 450° by UHVCVD to improve the nucleation of $Si_{1-x}Ge_x$ on SiO_2. Figure 3.18 shows plain-view TEM micrographs of the ELC poly-$Si_{0.77}Ge_{0.23}$ thin films. The laser energy density is 300mJ/cm^2 and the shot numbers per unit area is 100.

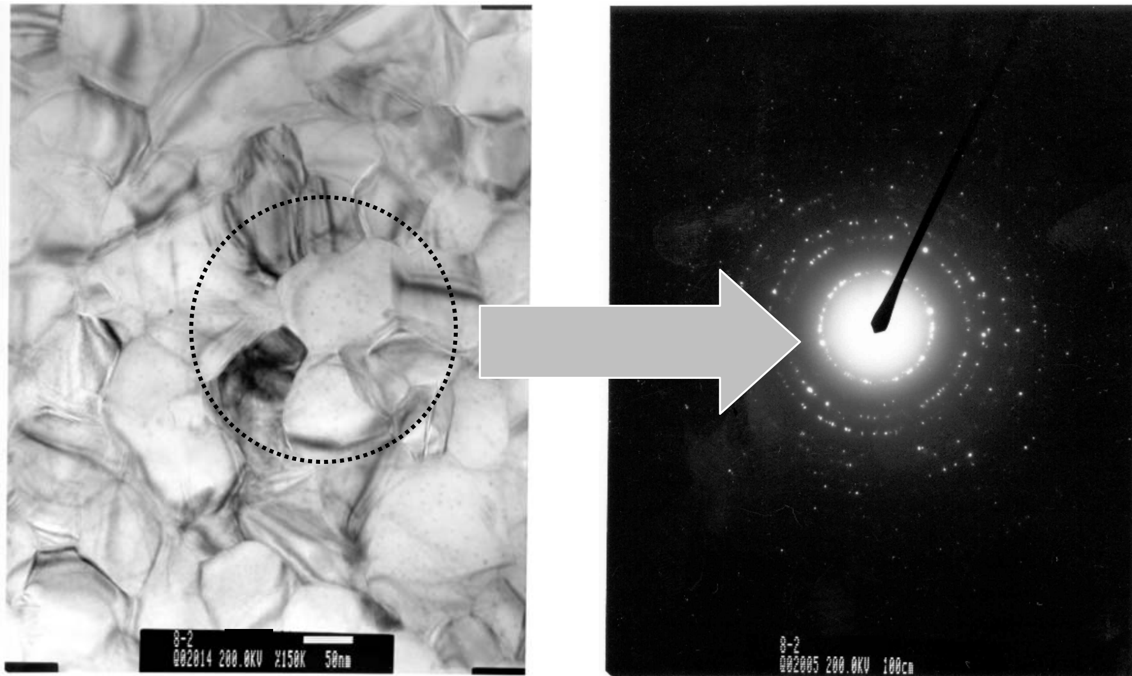

Figure 3.18(a). Plain-view TEM micrographs and diffraction pattern of the ELC poly-$Si_{0.77}Ge_{0.23}$ thin films. E = 300mJ/cm^2, 100 shots at R.T.

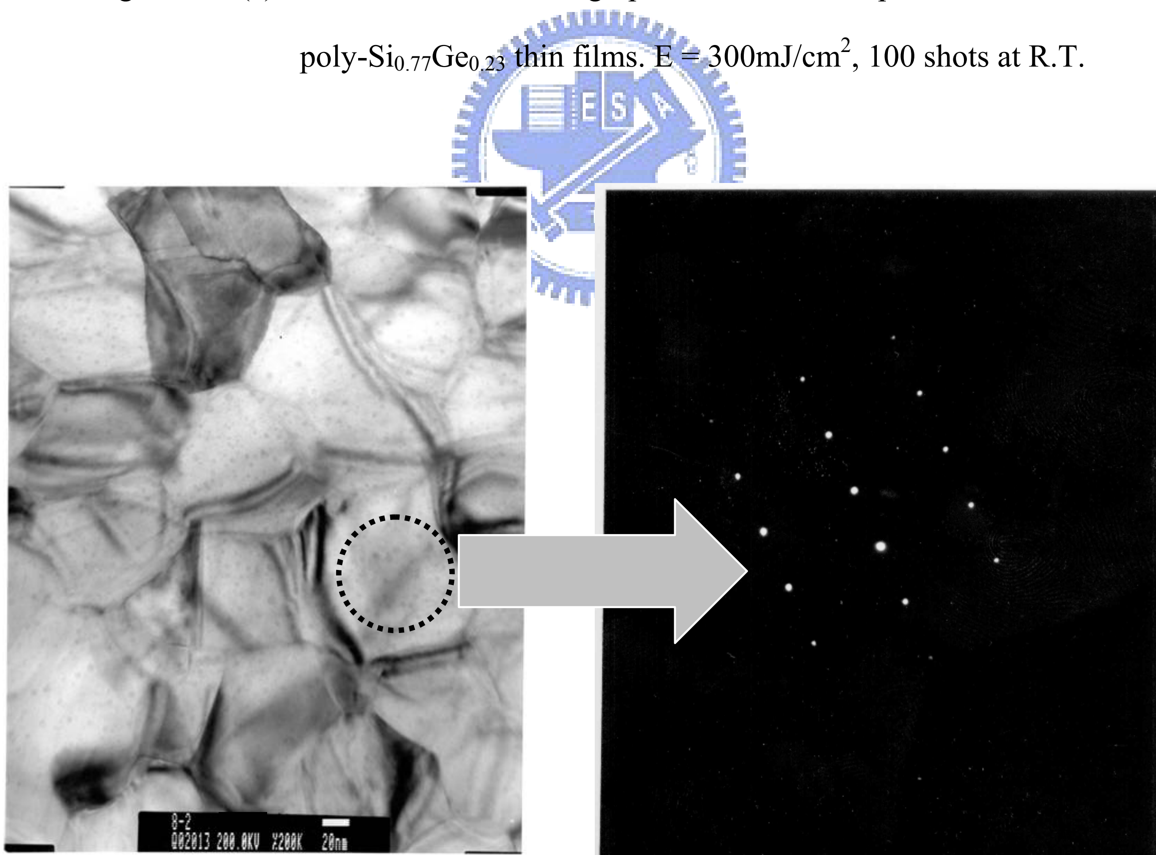

Figure 3.18(b). Plain-view TEM micrographs and diffraction pattern of the ELC poly-$Si_{0.77}Ge_{0.23}$ thin films. E = 300mJ/cm^2, 100 shots at R.T.

Elliptical-shaped grains are found in the ELC poly-$Si_{0.77}Ge_{0.23}$ thin films, which are similar to those of the ELC poly-Si thin films. Here it should be noted that the excimer laser energy is controlled in the partial melting regime. Therefore, the average grain size of the ELC poly-$Si_{0.77}Ge_{0.23}$ thin film is small. The electron diffraction pattern reveals a ring construction, which is the characteristic of polycrystalline structure. When the electron beam is shrunk to focus only on one grain, the electron diffraction pattern exhibits a clear dot pattern, which means the crystallinity inside the ELC poly-$Si_{0.77}Ge_{0.23}$ grain is pretty good.

Figure 3.19 displays the cross-section TEM images of the as-deposited and laser-crystallized poly-$Si_{0.77}Ge_{0.23}$ thin film. As depicted in cross-section TEM image, the as-deposited a-$Si_{0.77}Ge_{0.23}$ thin film reveals a uniform thickness and a smooth interface. The a-Si buffer layer can also be observed between the a-$Si_{0.77}Ge_{0.23}$ thin film and oxide substrate. On the other hand, as shown in Figure 3.19(b), a V-shaped, columnar crystalline structure is acquired for the poly-$Si_{0.77}Ge_{0.23}$ thin film after excimer laser irradiation. From the cross-section TEM image, the Ge segregation phenomenon mentioned in the AFM analysis is also found for the ELC poly-$Si_{0.77}Ge_{0.23}$ thin film deposited by UHVCVD. The energy dispersive X- ray (EDX) analysis was used to verify the atomic composition existing across the $Si_{0.77}Ge_{0.23}$ thin film. The EDX results indicated that the Ge atomic concentration near the film surface is higher than that in the middle of the film after excimer laser irradiation while the Si and Ge distribution is uniform across the whole film for the as-deposited a-$Si_{0.77}Ge_{0.23}$ thin film. This is consistent with the AES results, which illustrate the higher Ge atomic concentration near the film surface.

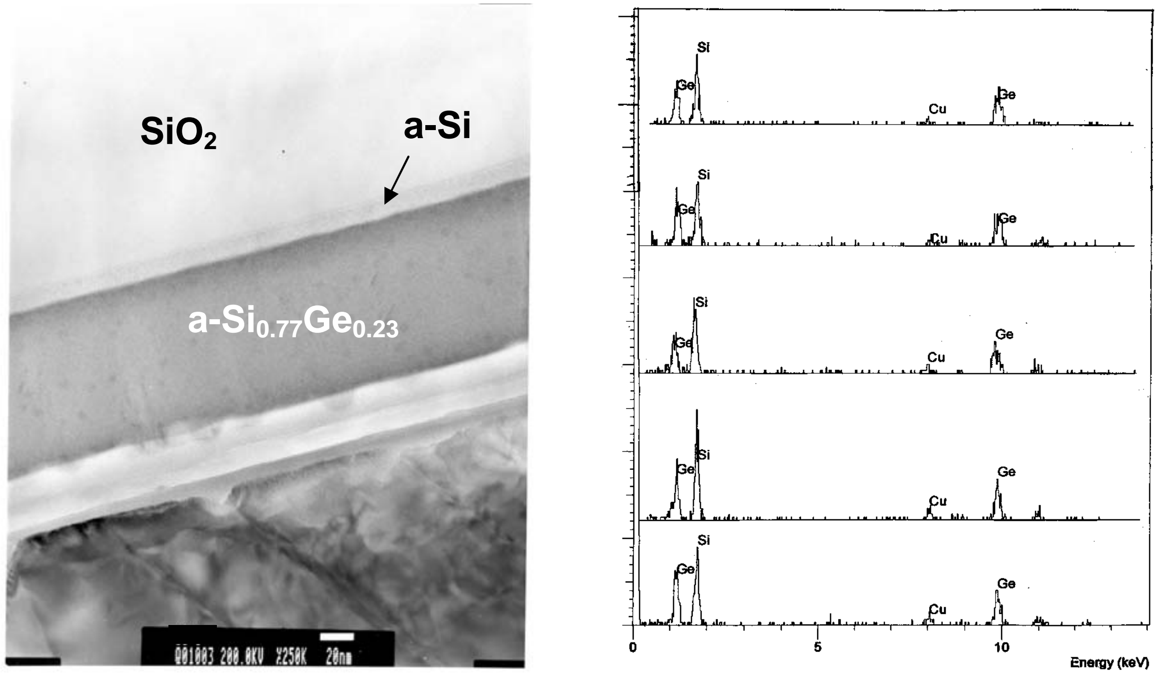

(a)

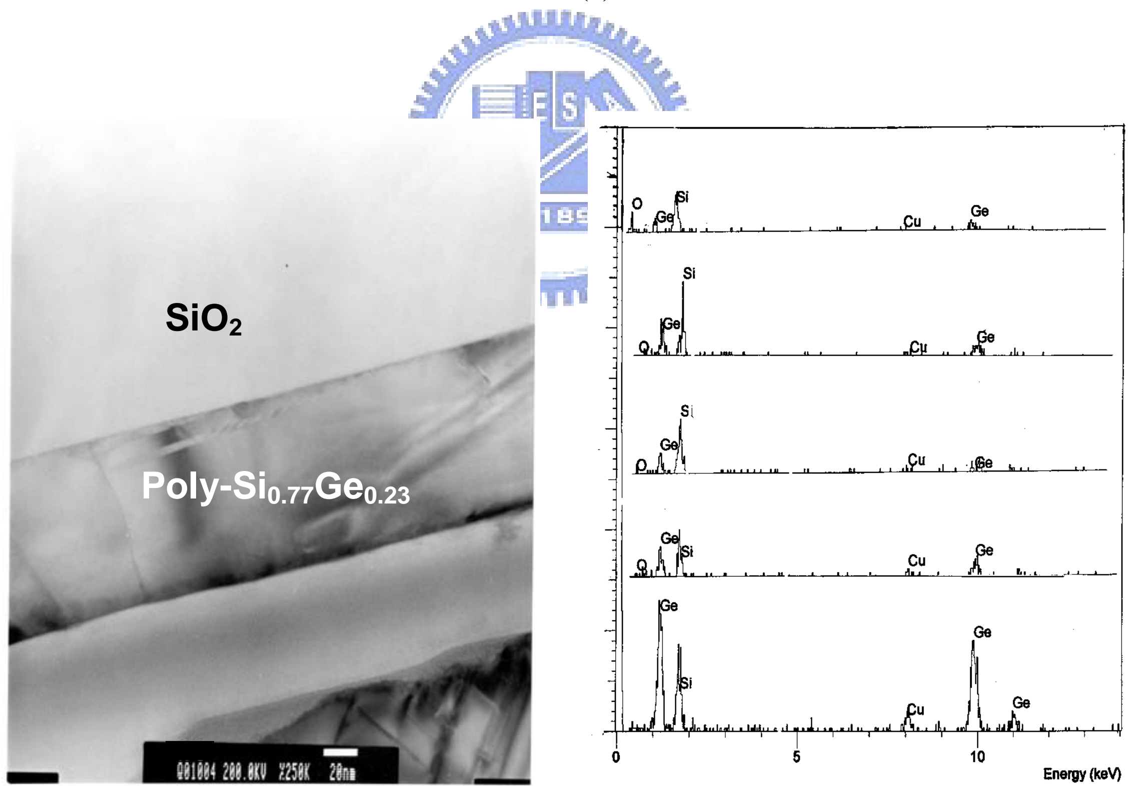

(b)

Figure 3.19. Cross-section TEM micrographs and EDX analysis results of the (a) as-deposited a-$Si_{0.77}Ge_{0.23}$ thin film.(b)ELC poly-$Si_{0.77}Ge_{0.23}$ thin film. E = 300mJ/cm^2, 100 shots at R.T.

3.3.2.5 Scanning Electron Microscope (SEM) Analysis

For device applications, the structure properties of the poly-Si thin films are of major interest. The primary concerns are the grain size, quality of the grains, and the grain size distribution, and these properties will strongly influence the electrical characteristics of TFT. In this work, the average grain size of the ELC poly-$Si_{1-x}Ge_x$ thin film is measured by using scanning electron microscopy (SEM). In order to distinguish the individual grain structure, before observation, the ELC poly-$Si_{1-x}Ge_x$ thin films are etched by using the Secco etching, which etched the grain boundaries more quickly than the interior parts of the grains. Figure 3.20 shows the SEM micrographs of the ELC poly-$Si_{1-x}Ge_x$ film after Secco etching. The excimer laser energy densities are adjusted to partially or completely melt the a-$Si_{1-x}Ge_x$ thin film. As shown in Figure 3.20, no distinguishable grains or grain boundaries are observed, instead of white ribbon-like regions covered on the film surface. From the previous AES and TEM analyses, it has been found that serious surface Ge segregation occurs after excimer laser irradiation. The white ribbon-like regions may be the segregated Ge-rich poly-$Si_{1-x}Ge_x$ layer remained at the film surface after Secco etch because the Secco etching solution is proven to be unable to etch the Ge-rich poly-$Si_{1-x}Ge_x$ thin film. To verify this assumption, the Secco etching process is modified with the adding of an NH_4OH-H_2O_2-H_2O solution followed by the original Secco etch solution. According to the previous reports, the Ge-rich poly-$Si_{1-x}Ge_x$ thin films can be etched effectively by using NH_4OH-H_2O_2-H_2O solution. Thus, after excimer laser irradiation, the poly-$Si_{1-x}Ge_x$ thin films are immersed in this solution to strip the Ge-rich region at first. After that, Secco etching is performed to etch the grain boundaries. Figure 3.21 ~ Figure 3.23 show the SEM images of the poly-$Si_{1-x}Ge_x$ thin film after the modified Secco etching process. As expected, the white ribbon-like regions are disappeared and the grain structures become apparent. Thus, it is undoubted that the white

ribbon-like regions at the film surface are the remained Ge-rich surface segregation layers. This again provides evidence that Ge atoms segregate toward the film surface in the ELC poly-$Si_{1-x}Ge_x$ thin film.

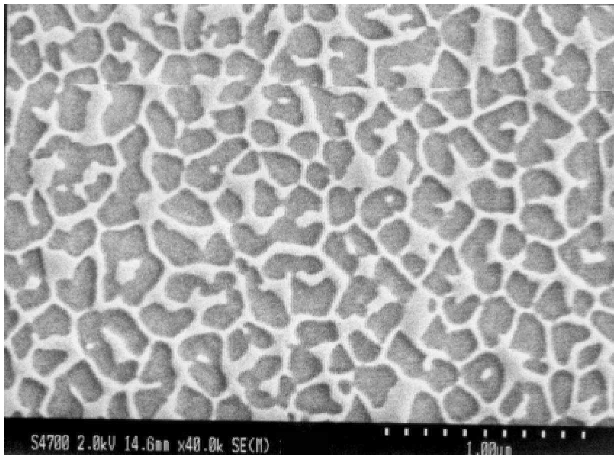

(a) 350 mJ/cm^2, 100 shots

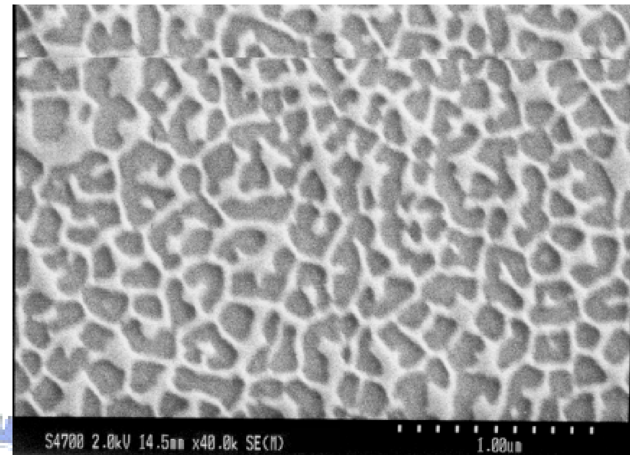

(b) E = 370 mJ/cm^2, 100 shots.

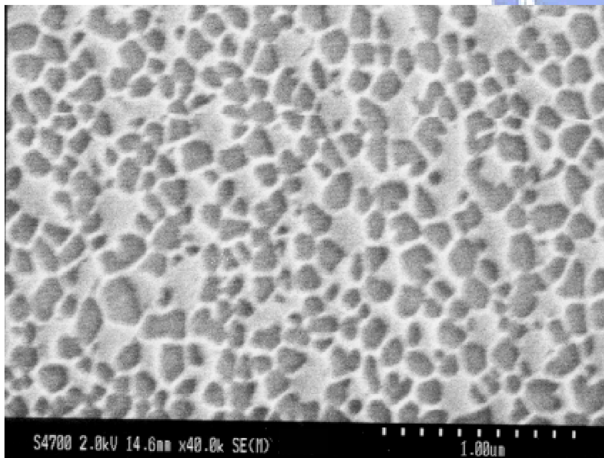

(c) 390 mJ/cm^2, 100 shots

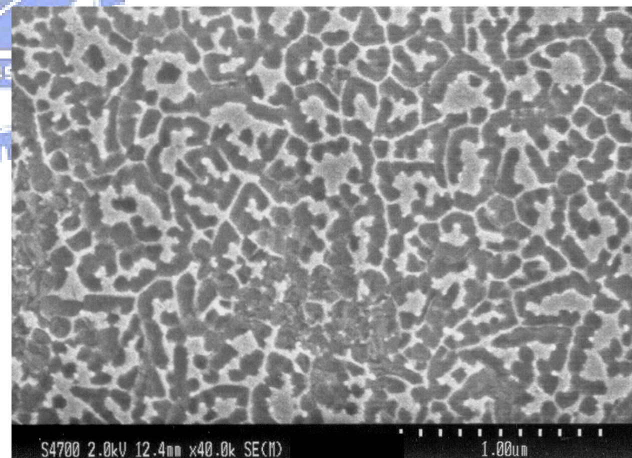

(d) 410 mJ/cm^2, 100 shots

Figure 3.20(a)-(d). The SEM micrographs of the ELC poly-$Si_{1-x}Ge_x$ film after Secco etching.

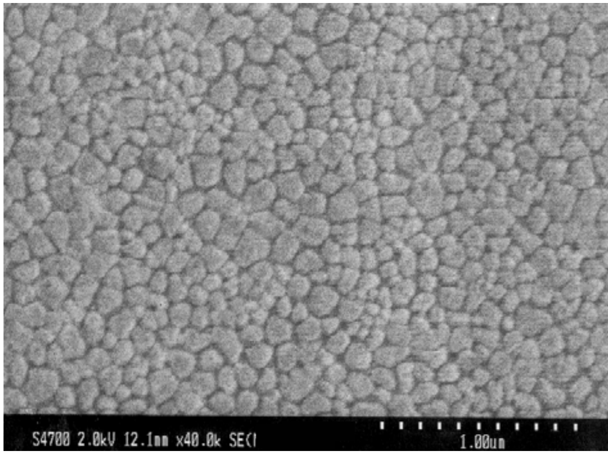

(a) 350mJ/cm^2, 100shots

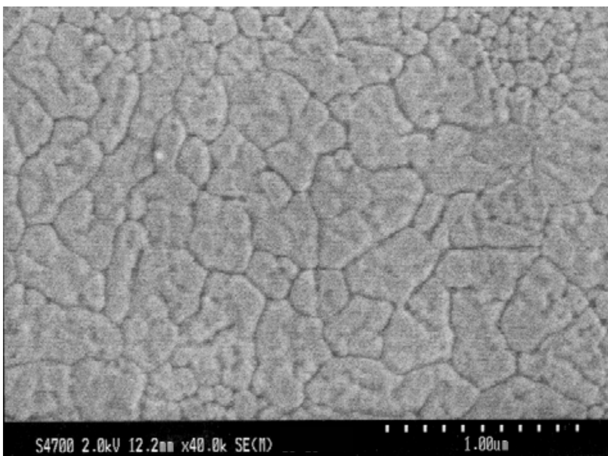

(b) 390mJ/cm^2, 100shots

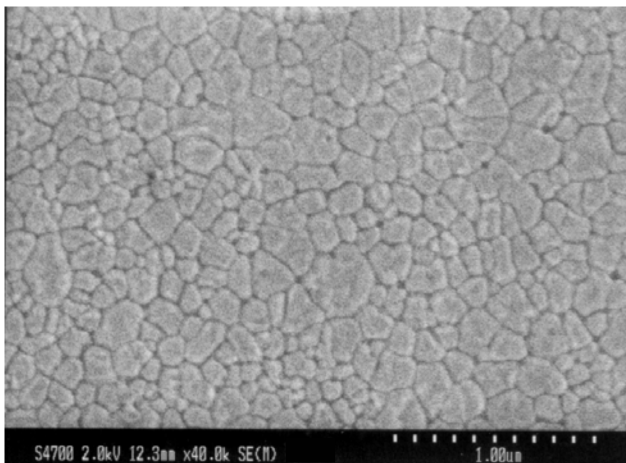

(c) 410mJ/cm^2, 100shots

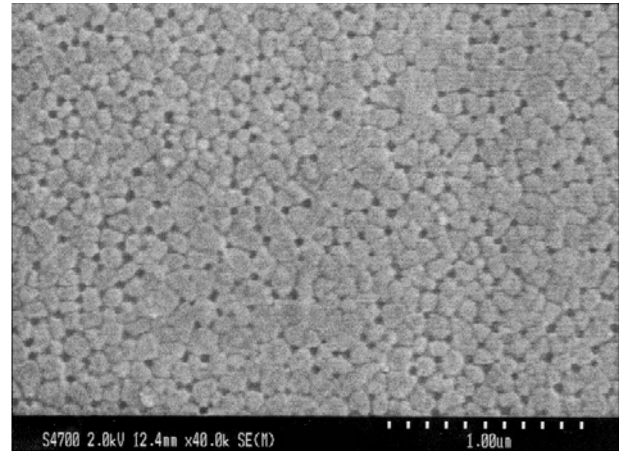

(d) 350mJ/cm^2, 20shots

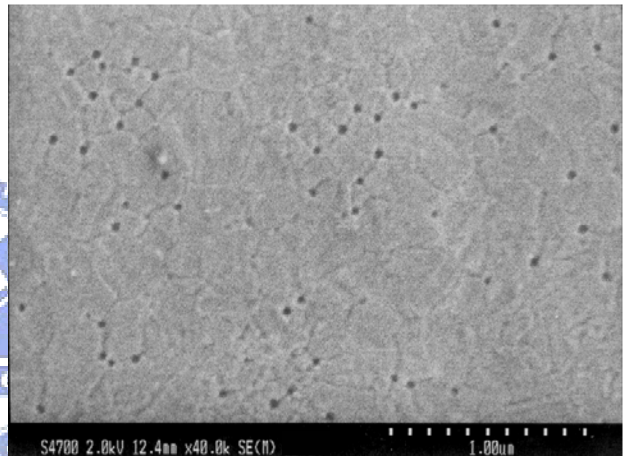

(e) 390mJ/cm^2, 20shots

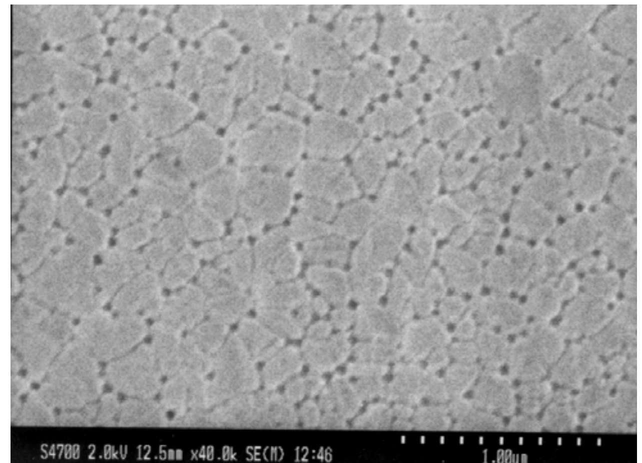

(f) 410mJ/cm^2, 20shots

Figure 3.21. SEM micrographs of ELC poly-$Si_{0.77}Ge_{0.23}$ films irradiated at R.T. after modified Secco etching treatment.